Linear and nonlinear traveling edge waves in optical honeycomb lattices

Mark J. Ablowitz,[1] Christopher W. Curtis,[2] and Yi-Ping Ma[1]

[1]*Department of Applied Mathematics, University of Colorado, Boulder, Colorado 80309, USA*
[2]*Department of Mathematics and Statistics, San Diego State University, San Diego, California 92182, USA*

Traveling unidirectional localized edge states in optical honeycomb lattices are analytically constructed. They are found in honeycomb arrays of helical waveguides designed to induce a periodic pseudomagnetic field varying in the direction of propagation. Conditions on whether a given pseudofield supports a traveling edge mode are discussed; a special case of the pseudofields studied agrees with recent experiments. Interesting classes of dispersion relations are obtained. Envelopes of nonlinear edge modes are described by the classical one-dimensional nonlinear Schrödinger equation along the edge. Nonlinear states termed edge solitons are predicted analytically and are found numerically.

I. INTRODUCTION

Substantial attention has been paid to the understanding of edge modes in both condensed-matter physics and optics. Interest in such modes goes back to the first studies of the quantum Hall effect where it was found that the edge current was quantized [1–3]. There has also been interesting research on the connection of the existence of edge states to the geometry of eigenspaces of Schrödinger operators [4–9]. Recently, theoretical results gave support to the possible existence of unidirectional modes in optical honeycomb (HC) lattices [10,11]. Due to the extra symmetry of the honeycomb lattice, Dirac points, or conical intersections between dispersion bands, exist. The unidirectional modes in Refs. [10,11] emerged due to symmetry-breaking perturbations which separated the Dirac points and induced a nontrivial integer "topological" charge on the separated bands.

The first experimental realization of unidirectional electromagnetic edge modes was in Ref. [12]. These results relied on magnetic-field effects and were carried out in the microwave regime. Furthermore, the modes were found on a square lattice which have no associated Dirac points. However, in recent work, it was experimentally shown in Ref. [13] that by introducing a symmetry-breaking pseudomagnetic field into a honeycomb optical lattice, the Dirac points separate, and unidirectional edge wave propagation at optical frequencies occurs. These edge waves are shown to be effectively immune to backscattering from obstacles and so represent a new degree of control of light.

Such pseudomagnetic fields are generated by a periodic change in the index of refraction of the waveguides in the direction of propagation. Considering the direction of the wave propagation as "time," the variation in the index of refraction has a well-defined helicity and thus breaks time-reversal symmetry [13]. To model this effect in a honeycomb optical lattice, we begin with the lattice nonlinear Schrödinger (NLS) equation [13] with cubic Kerr contribution,

$$i\,\partial_z\psi = -\frac{1}{2k_0}\nabla^2\psi + \frac{k_0\,\Delta n}{n_0}\psi - \gamma|\psi|^2\psi. \quad (1)$$

Here k_0 is the input wave number, n_0 is the ambient refractive index, $\Delta n/n_0$ is the linear index change relative to n_0, also referred to as the potential, and γ represents the nonlinear

index contribution. The complex scalar field ψ is the envelope of the electric field, z is the direction of propagation and takes on the role of time, (x,y) is the transverse plane, and $\nabla \equiv (\partial_x,\partial_y)$. In Ref. [13], the potential Δn is taken to be a two-dimensional (2D) lattice potential defined on the (x,y) plane moving along a prescribed path in the z direction. This motion is characterized by a path function $\mathbf{a}(z) = (a_1(z),a_2(z))$ such that after the coordinate transformation,

$$x' = x - a_1(z), \quad y' = y - a_2(z), \quad z' = z,$$

the transformed potential $\Delta n = \Delta n(x',y')$ is independent of z'.

Experimentally, the path represented by $\mathbf{a}(z)$ can be written into the optical material (e.g., fused silica) via the femtosecond laser-writing technique [14], which was the method used in Ref. [13]. Since this technique enables waveguides to be written along general paths, we only require $\mathbf{a}(z)$ to be a smooth function. Introducing a transformed field,

$$\psi = \tilde{\psi}\,\exp\left[\frac{i}{2k_0}\int_0^z|\mathbf{A}(\xi)|^2 d\xi\right],$$

where $\mathbf{A}$ is induced by the path function $\mathbf{a}$ via the formula,

$$\mathbf{A}(z) = -k_0\mathbf{a}'(z), \quad (2)$$

we transform Eq. (1) to

$$i\,\partial_{z'}\tilde{\psi} = -\frac{1}{2k_0}(\nabla' + i\mathbf{A}(z'))^2\tilde{\psi} + \frac{k_0\,\Delta n}{n_0}\tilde{\psi} - \gamma|\tilde{\psi}|^2\tilde{\psi}. \quad (3)$$

In these coordinates, $\mathbf{A}$ appears in the same way as if we had added a magnetic field to Eq. (1), and so we call $\mathbf{A}$ a pseudomagnetic field. Taking l to be the lattice scale size, we employ the dimensionless coordinates $x' = lx$, $y' = ly$, and $z' = 2k_0l^2z$. We introduce the scaled field $\tilde{\psi} = \sqrt{P_*}\psi$, where P_* is the input peak power, and by rescaling $\mathbf{A}$ accordingly and defining $V(\mathbf{r}) = 2k_0^2l^2\Delta n/n_0$ where $\mathbf{r} \equiv (x,y)$, we get the normalized lattice NLS equation,

$$i\,\partial_z\psi = -(\nabla + i\mathbf{A}(z))^2\psi + V(\mathbf{r})\psi - \sigma_0|\psi|^2\psi. \quad (4)$$

The dimensionless coefficient $\sigma_0 = 2\gamma k_0l^2P_*$ is the strength of the nonlinear change in the index of refraction. We also note that for convenience, the dimensionless variables x, y, z, and ψ are used; these dimensionless variables should not be

confused with the dimensional variables in Eq. (1). In this paper we take the potential $V(\mathbf{r})$ to be of HC type.

It is interesting to note that in condensed-matter physics Eq. (4) with $\sigma_0 = 0$ describes Bloch electrons in a homogeneous electric field [15] where the electric field is proportional to the time derivative of the vector potential $\mathbf{A}$. Thus, although the parameter regime addressed in this paper is chosen to be consistent with experiments performed on optical graphene in Ref. [13], the basic asymptotic theory described in this paper applies to different and important physical phenomena.

In Ref. [13], in terms of normalized coordinates, the particular helical pseudomagnetic field,

$$\mathbf{A}(z) = (A_1(z), A_2(z)) = \kappa(\sin \Omega z, -\cos \Omega z), \quad (5)$$

where κ and Ω are constant, was studied numerically and experimentally. Numerically calculated dispersion relations of the associated discrete wave problem, obtained after employing the tight-binding approximation, are given which indicate the existence of unidirectional edge modes. Motivated by the work in Refs. [13,16], we analytically investigate the existence of unidirectional traveling edge modes. This is performed for general periodic pseudofields $\mathbf{A}(z)$ which includes Eq. (5) as a subcase. By allowing the pseudofield to evolve relatively rapidly, which is consistent with the experiments in Ref. [13] and by using Floquet theory (cf. Refs. [17,18]), an asymptotic theory is developed which leads to explicit formulas describing how the dispersion relation depends on a given pseudofield $\mathbf{A}(z)$. Therefore, we can theoretically predict for general pseudofields when unidirectional modes exist.

To exemplify the different dispersion relations allowed by our analysis, we generalize the helical motion in Eq. (5) to include one additional trigonometric term,

$$A_1(z) = \kappa \sin \Omega z + \lambda \sin (D\Omega z + \phi),$$
$$A_2(z) = -\kappa \cos \Omega z + \lambda \cos (D\Omega z + \phi),$$

where D is taken to be 1 or 2, λ is constant, and we take $\phi = \pi/4$. The values of κ, λ, and ϕ are related to the amplitude of the first harmonic, additional harmonic, and phase offset, respectively, of the additional harmonic. Since $\mathbf{A}(z)$ is given by Eq. (2), in principle, for every $\mathbf{a}(z)$ written into the optical lattice, each of the terms κ, λ, and ϕ can be controlled via the laser-writing procedure. Within this extended family of pseudofields, we analytically find dispersion relations of the same form that were found in Ref. [13] as well as additional classes of dispersion relations. In terms of wave propagation, we find that in addition to nearly unidirectional wave propagation, there are cases with significant dispersion. Thus, not every symmetry-breaking pseudofield generates coherent unidirectional modes.

We are also able to analyze the effect of nonlinearity on these traveling edge modes. The classical one-dimensional (1D) nonlinear Schrödinger equation governing the envelope of the edge modes is derived below and is found to be an effective description of nonlinear traveling edge modes. Using this equation, we find analytically and confirm numerically that the unidirectionality of waves is maintained in the case of soliton propagation. In the focusing NLS evolution, the nonlinearity balances dispersion to produce nonlinear edge solitons.

Depending on the choice of parameters, some of the nonlinear modes appear to be immune to backscattering, and they are in the topologically protected regime predicted by linear theory, cf. Ref. [13]. This indicates that unidirectional nonlinear edge modes should be observable. These results hint at a new means for the control of light conferred by merging nonlinear and symmetry-breaking effects. See also Ref. [19] where bulk nonlinear modes have been found. Furthermore, such "topologically protected nonlinear states" can apply to other systems, e.g., recently introduced one-dimensional domain walls [20].

II. PRELIMINARIES

To begin the analysis, the substitution $\psi = e^{-i\mathbf{r} \cdot \mathbf{A}(z)}\phi$ in Eq. (4) gives

$$i \, \partial_z \phi = -\Delta \phi - \mathbf{r} \cdot \mathbf{A}_z \phi + V(\mathbf{r})\phi - \sigma_0 |\phi|^2 |\phi. \quad (6)$$

The tight-binding approximation for large V assumes a Bloch wave envelope of the form [21]

$$\phi \sim \sum_{\mathbf{v}} (a_{\mathbf{v}}(z)\phi_{1,\mathbf{v}} + b_{\mathbf{v}}(z)\phi_{2,\mathbf{v}})e^{i\mathbf{k}\cdot\mathbf{v}}, \quad (7)$$

where $\phi_{1,\mathbf{v}} = \phi_1(\mathbf{r} - \mathbf{v})$, $\phi_{2,\mathbf{v}} = \phi_2(\mathbf{r} - \mathbf{v})$ are the linearly independent orbitals associated with the two sites A and B where the honeycomb potential $V(\mathbf{r})$ has minima in each fundamental cell and $\mathbf{k}$ is a vector in the Brillouin zone. Each $\mathbf{v} = m\mathbf{v}_1 + n\mathbf{v}_2$ where the period vectors $\mathbf{v}_1$ and $\mathbf{v}_2$ are given by

$$\mathbf{v}_1 = (\sqrt{3}/2, 1/2), \quad \mathbf{v}_2 = (\sqrt{3}/2, -1/2).$$

Figure 1 shows the semi-infinite honeycomb lattice with zigzag boundary conditions studied in this paper. The indexing scheme for the A and B sites follows [22]. For each site $\{A, B\}_{m,n}$, the subscripts m and n denote the infinite and semi-infinite directions, respectively. The zigzag boundary conditions require $n \geq 0$ for $B_{m,n}$ and $n \geq 1$ for $A_{m,n}$, whereas $m \in \mathbb{Z}$ for both. The honeycomb lattice is formed by those sites with $m + n$ even, but to facilitate the computation we carry out the analysis for the entire semi-infinite lattice in the (m,n) plane. In addition to the primitive lattice vectors $\mathbf{v}_1$ and $\mathbf{v}_2$, Fig. 1 also shows the vectorial distance $\mathbf{d}$ between two adjacent sites $A_{m,n}$ and $B_{m,n}$. It can be seen that $\mathbf{d} = (1/\sqrt{3}, 0)$ for a perfect honeycomb lattice. Substituting the tight-binding
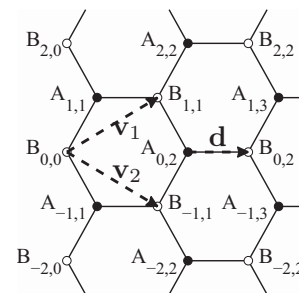

FIG. 1. The semi-infinite honeycomb lattice with zigzag boundary conditions. The A and B sites are indexed following Ref. [22]. The primitive lattice vectors $\mathbf{v}_1$ and $\mathbf{v}_2$ and the intersite distance $\mathbf{d}$ are also labeled.

approximation (7) into Eq. (6), carrying out the requisite calculations (see Ref. [21] for more details) and after dropping small terms and renormalizing, we arrive at the following 2D discrete system,

$$i \, \partial_z a_{mn} + e^{i\mathbf{d}\cdot\mathbf{A}}(\mathcal{L}_-(z)b)_{mn} + \sigma|a_{mn}|^2 a_{mn} = 0, \quad (8)$$

$$i \, \partial_z b_{mn} + e^{-i\mathbf{d}\cdot\mathbf{A}}(\mathcal{L}_+(z)a)_{mn} + \sigma|b_{mn}|^2 b_{mn} = 0, \quad (9)$$

where

$$(\mathcal{L}_- b)_{mn} = b_{mn} + \rho(b_{m-1,n-1}e^{-i\theta_1} + b_{m+1,n-1}e^{-i\theta_2}),$$
$$(\mathcal{L}_+ a)_{mn} = a_{mn} + \rho(a_{m+1,n+1}e^{i\theta_1} + a_{m-1,n+1}e^{i\theta_2}),$$

ρ is a lattice deformation parameter, $\theta_1(z) = \mathbf{v}_1 \cdot (\mathbf{k} + \mathbf{A}(z))$, $\theta_2(z) = \mathbf{v}_2 \cdot (\mathbf{k} + \mathbf{A}(z))$, and σ is a constant which depends on σ_0 and the underlying orbitals. Taking a discrete Fourier transform in m, i.e., letting $a_{mn} = a_n e^{im\omega}$ and $b_{mn} = b_n e^{im\omega}$, yields the simplified system,

$$i \, \partial_z a_n + e^{i\mathbf{d}\cdot\mathbf{A}}(b_n + \rho\gamma^*(z;\omega)b_{n-1}) + \sigma|a_n|^2 a_n = 0, \quad (10)$$

$$i \, \partial_z b_n + e^{-i\mathbf{d}\cdot\mathbf{A}}(a_n + \rho\gamma(z;\omega)a_{n+1}) + \sigma|b_n|^2 b_n = 0, \quad (11)$$

where $\gamma(z;\omega) = 2e^{i\varphi_+(z)}\cos(\varphi_-(z) - \omega)$ with

$$\varphi_+(z) = (\theta_2(z) + \theta_1(z))/2, \quad \varphi_-(z) = (\theta_2(z) - \theta_1(z))/2.$$

III. LINEAR THEORY

In this section we omit the nonlinear terms by setting $\sigma = 0$; the nonlinear case is discussed in Sec. V. The theory we develop is based upon the normalized frequency of the pseudofield being large, which is consistent with the experimental parameters used in Ref. [13]. This leads to an analytical formulation in which we can express the linear-dispersion relation explicitly in terms of integrals which are readily computed. The details of the asymptotic method are reserved for Appendix A; here we only give the main formulas.

Since we assume that the pseudomagnetic field varies rapidly, we express it as $\mathbf{A} = \mathbf{A}(\zeta)$ where $\zeta = \epsilon^{-1}z$, $|\epsilon| \ll 1$. Employing the method of multiple scales [23], we write the vectors a and b as functions of the fast and slow scales ζ, z and expand so that the nth components of each vector are given by

$$a_n = a_n(z, \zeta) = a_n^{(0)} + O(\epsilon), \quad b_n = b_n(z, \zeta) = b_n^{(0)} + O(\epsilon).$$

We apply zigzag boundary conditions, which implies $a_n = 0$, $n \leqslant 0$. The asymptotic method in Appendix A shows that at leading order we have a mode which is nearly stationary; it is given by

$$a_n^{(0)} = 0, \quad b_n^{(0)} = C(Z)b_n^S, \quad b_n^S = (-\bar{\vartheta}/\bar{\varrho})^n,$$

where

$$\varrho(\zeta) = e^{i\mathbf{d}\cdot\mathbf{A}}, \quad \vartheta(\zeta;\omega) = \vartheta_c(\zeta)\cos\omega + \vartheta_s(\zeta)\sin\omega,$$
$$\vartheta_c(\zeta) = \varrho(\zeta)2\rho e^{-i\varphi_+}\cos\varphi_-,$$
$$\vartheta_s(\zeta) = \varrho(\zeta)2\rho e^{-i\varphi_+}\sin\varphi_-,$$

and the average $\bar{f}$ means

$$\bar{f} \equiv T^{-1}\int_0^T f(\zeta)d\zeta,$$

where T is the period of $\mathbf{A}$.

The asymptotic method further yields

$$C(Z) = C(0)\exp(-i\tilde{\alpha}(\omega)Z), \quad (12)$$

where the dispersion relation $\tilde{\alpha}$ is real and is given explicitly as a function of the pseudomagnetic field $\mathbf{A}(\zeta)$ by

$$\tilde{\alpha}(\omega) = -\frac{i}{T}\int_0^T \int_0^\zeta Q(\zeta';\omega)Q^*(\zeta;\omega)d\zeta'd\zeta, \quad (13)$$

with

$$Q(\zeta;\omega) = -\varrho(\zeta)\frac{\bar{\vartheta}}{\bar{\varrho}} + \vartheta(\zeta;\omega). \quad (14)$$

To have localized modes, we need $|\bar{\vartheta}/\bar{\varrho}| < 1$, namely,

$$P(\omega) \equiv |\bar{\vartheta}/\bar{\varrho}|^2 = P_0 + P_c\cos 2\omega + P_s\sin 2\omega < 1, \quad (15)$$

where

$$P_0 = \frac{1}{2}\frac{|\bar{\vartheta}_c|^2 + |\bar{\vartheta}_s|^2}{|\bar{\varrho}|^2},$$

$$P_c = \frac{1}{2}\frac{|\bar{\vartheta}_c|^2 - |\bar{\vartheta}_s|^2}{|\bar{\varrho}|^2},$$

$$P_s = \frac{1}{2}\frac{\bar{\vartheta}_c\bar{\vartheta}_s^* + \bar{\vartheta}_c^*\bar{\vartheta}_s}{|\bar{\varrho}|^2}.$$

The interval of localization $\mathcal{I}$, a subset of the circle $S^1 = \mathbb{R}/(\pi\mathbb{Z})$, can be determined from Eq. (15). There are three qualitatively different scenarios,

$$\text{(I): } \sqrt{P_c^2 + P_s^2} < 1 - P_0, \quad P_0 < 1,$$

$$\text{(II): } \sqrt{P_c^2 + P_s^2} > |P_0 - 1|,$$

$$\text{(III): } \sqrt{P_c^2 + P_s^2} < P_0 - 1, \quad P_0 > 1.$$

In case (II), there are two values of ω determined by $|\bar{\vartheta}/\bar{\varrho}| = 1$, say $\omega_\pm$, at which localized modes delocalize. Thus at $\omega_\pm$, the edge band is emitted from the bulk spectrum, and so $\mathcal{I} = (\omega_-, \omega_+)$. In case (I), $\omega_\pm$'s drift apart so that $\mathcal{I} = S^1$, whereas in case (III) they come together so that $\mathcal{I} = \varnothing$.

Letting $Q(\zeta;\omega) = Q_c(\zeta)\cos\omega + Q_s(\zeta)\sin\omega$, Eq. (13) becomes

$$\tilde{\alpha}(\omega) = \tilde{\alpha}_0 + \tilde{\alpha}_c\cos 2\omega + \tilde{\alpha}_s\sin 2\omega, \quad (16)$$

where one finds directly that $\tilde{\alpha}_0$, $\tilde{\alpha}_c$, and $\tilde{\alpha}_s$ can be written in terms of double integrals. It follows from Eq. (16) that the number of times N that $\tilde{\alpha}(\omega)$ crosses $\tilde{\alpha} = 0$ on $\mathcal{I}$ can only be $N = 0$, 1, or 2. For $N = 0$ or $N = 2$, it is possible for edge states to exist in pairs which allow propagation in different directions. In this case, the edge modes are susceptible to dispersion. When $N = 1$, though, because of the unique root of $\tilde{\alpha}$, we expect to find unidirectional edge modes that exhibit essentially no dispersion.

We note that the expressions for the localization interval $\mathcal{I}$ and the dispersion relation $\tilde{\alpha}(\omega)$ are invariant under the constant translations,

$$(\omega, \mathbf{A}(\zeta)) \to (\omega + (\mathbf{v}_1 - \mathbf{v}_2)\cdot\bar{\mathbf{A}}/2, \mathbf{A}(\zeta) - \bar{\mathbf{A}}),$$

$$(\mathbf{k}, \mathbf{A}(\zeta)) \to (0, \mathbf{A}(\zeta) + \mathbf{k}),$$

where $\bar{\mathbf{A}}$ is an arbitrary constant 2D vector. Hence without loss of generality we will consider $\mathbf{A}(\zeta)$ with zero mean and set $\mathbf{k} = 0$ in the following.

In this paper the lattice deformation parameter ρ is taken to be positive. As shown in Appendix B, in the tight-binding limit ρ can be tuned to any positive value by slightly deforming a perfect honeycomb potential. Since both $P(\omega)$ and $\tilde{\alpha}(\omega)$ are proportional to ρ^2 as ρ is decreased with the other parameters fixed, the localization interval $\mathcal{I}$ is broadened, and the group velocity $\tilde{\alpha}'(\omega)$ is decreased.

Now let us assume that $\mathbf{A}$ possesses the threefold symmetry [see Figs. 4(a)–4(c) for examples], i.e.,

$$\mathbf{A}(\zeta + 2\pi/3) = R_{2\pi/3}\mathbf{A}(\zeta), \tag{17}$$

where $R_{2\pi/3}$ denotes rotation by $2\pi/3$. As shown in Appendix B, in the tight-binding limit we have the approximation $\mathbf{d} = (1/\sqrt{3}, 0)$ independent of ρ. Using the identities $\mathbf{d} - \mathbf{v}_1 = R_{2\pi/3}^{-1}\mathbf{d}$ and $\mathbf{d} - \mathbf{v}_2 = R_{2\pi/3}\mathbf{d}$, we can simplify the off-diagonal element ϑ of the matrix $\mathcal{L}^-$ as

$$\vartheta(\zeta; \omega) = \rho(e^{-i\omega}\varrho(\zeta_+) + e^{i\omega}\varrho(\zeta_-)), \tag{18}$$

where $\zeta_\pm = \zeta \pm 2\pi/3$. It then follows that

$$\bar{\vartheta}/\bar{\varrho} = \rho(e^{-i\omega} + e^{i\omega}), \tag{19}$$

so the localization interval $\mathcal{I}$ depends only on ρ as

$$\mathcal{I} = \begin{cases} [\cos^{-1}(1/(2\rho)), \pi - \cos^{-1}(1/(2\rho))], & \rho \geqslant 1/2, \\ S^1, & \rho < 1/2. \end{cases}$$

This expression for $\mathcal{I}$ is identical to the one derived in Ref. [22] in the absence of the pseudofield $\mathbf{A}$.

IV. CLASSIFICATION OF THE DISPERSION RELATION

To make this analysis more concrete, we take the periodic pseudofield to be

$$\mathbf{A}(\zeta) = \kappa(s(\zeta), -c(\zeta)) + \lambda(s(D\zeta + \phi), c(D\zeta + \phi)).$$

Here, $s(\zeta) = \sin\zeta$, $c(\zeta) = \cos\zeta$, and $\zeta = z/\epsilon$. Unless otherwise stated, we set $\epsilon = 1.5/(2\pi)$, which is motivated by experiments [13]. This pseudofield is characterized by three continuous parameters κ, λ, and ϕ, and a discrete parameter $D \in \mathbb{Z}$. It can be seen that $\mathbf{A}(\zeta)$ has a $(D+1)$-fold symmetry; in particular, $\mathbf{A}(\zeta)$ has the threefold symmetry given by Eq. (17) when $D = 3n - 1$, $n \in \mathbb{Z}$. In the following we fix $\phi = \pi/4$ and explore $D = 2$ and $D = 1$.

Figure 2 shows the (κ, λ) plane, hereafter referred to as the phase diagram, partitioned based on our asymptotic theory according to all possible combinations of cases (I)–(III) and $N = 0$–2, hereafter denoted by (case, N). All six combinations have been found. Figure 3 shows the full dispersion relations, or Floquet parameters, $\alpha(\omega) = \epsilon\tilde{\alpha}(\omega)$ at representative points (a)–(f) on the (κ, λ) plane in Fig. 2 computed directly using Eqs. (10) and (11). The numerical computations are performed using a finite number of lattice sites with zigzag boundary conditions on both ends. Unless otherwise stated, each vector a and b is defined over 20 lattice sites to allow for sufficient decay. The dark black curves in Fig. 3 show Eq. (16). It can be seen that the asymptotic theory describes the dispersion relation of edge modes almost exactly in all cases studied.
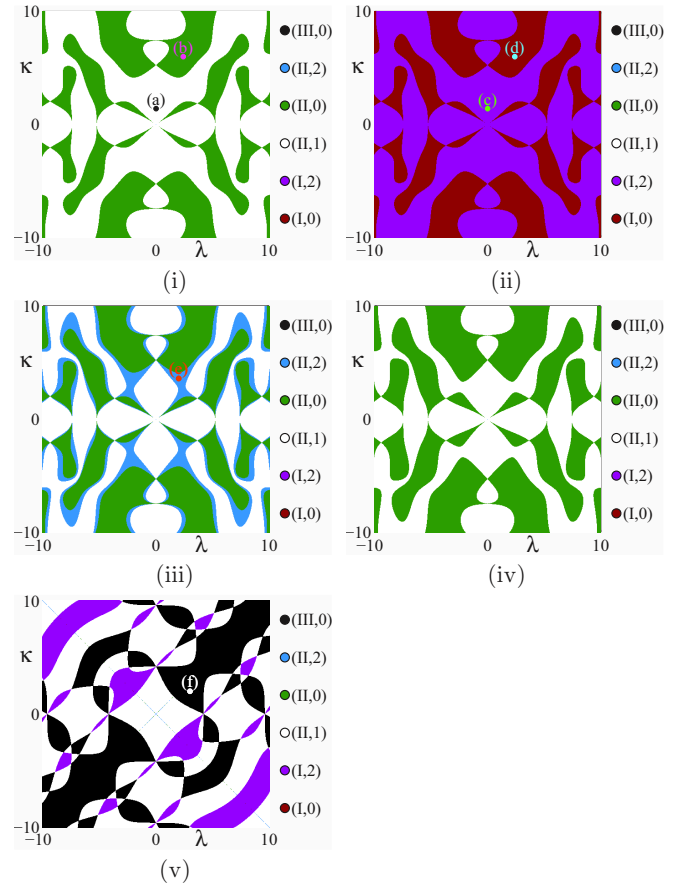

FIG. 2. (Color online) The (κ, λ) plane partitioned according to the combinations of cases (I)–(III) and $N = 0$–2, represented as (case, N) pairs with parameters (ρ, D): (i) (1,2), (ii) (0.4,2), (iii) (0.6,2), (iv) (2,2), and (v) (1,1). The full dispersion relations at the labeled points (a)–(f) are shown in Fig. 3.

Figure 4 shows the pseudofield $\mathbf{A}$ with the parameters used in Fig. 3.

The phase diagrams in Figs. 2(i)–2(iv) are computed using a threefold symmetric pseudofield ($D = 2$). Thus at $\rho = 1$ [Fig. 2(i)], we have case (II) with the localization interval $\mathcal{I} = (\pi/3, 2\pi/3)$. In this case the phase diagram is partitioned into $N = 1$ and $N = 0$ regions. In Fig. 3(a), using a pseudofield with a single harmonic [Fig. 4(a)] as in Ref. [13], we obtain an $N = 1$ dispersion curve with a nonzero slope. This indicates that the linear edge mode propagates as in Ref. [13]. In Fig. 3(b), using a pseudofield with a nonzero second harmonic [Fig. 4(b)], we obtain an $N = 0$ dispersion curve that does not connect between the upper and the lower bulk dispersion branches.

At $\rho = 0.4 < 1/2$ [Fig. 2(ii)], we have case (I) with $\mathcal{I} = S^1$. In this case the phase diagram is partitioned into $N = 2$ and $N = 0$ regions. Interestingly, these regions appear to coincide with the $N = 1$ and $N = 0$ regions, respectively, in the $\rho = 1$ case. In Figs. 3(c) and 3(d) using the same pseudofields as in Figs. 3(a) and 3(b), respectively, we observe that a pseudofield with a single harmonic gives $N = 2$, but a nonzero second harmonic results in $N = 0$.
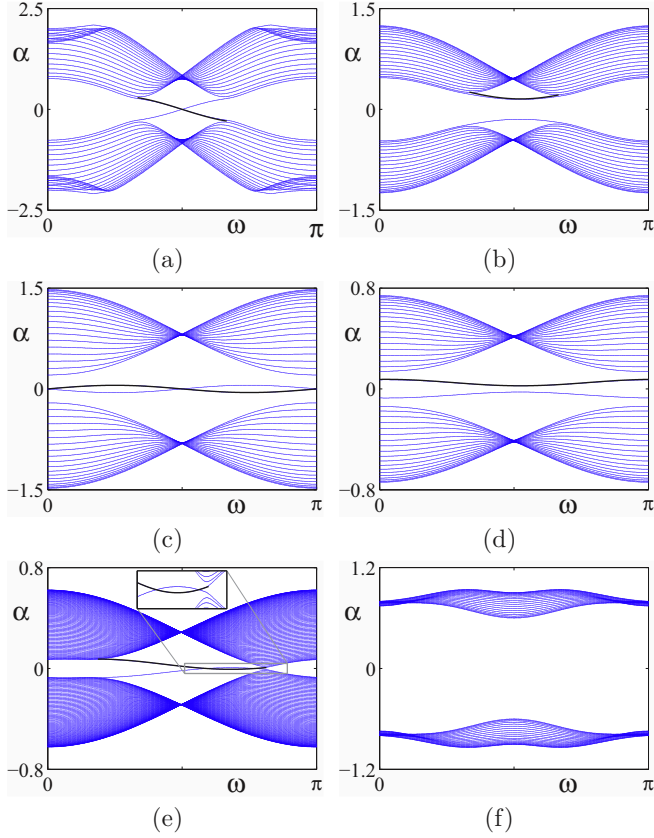
FIG. 3. (Color online) Dispersion relations for points in Fig. 2 with parameters $(\rho, D, \kappa, \lambda)$: (a) $(1,2,1.4,0)$, (b) $(1,2,6,2.4)$, (c) $(0.4,2,1.4,0)$, (d) $(0.4,2,6,2.4)$. (e) $(0.6,2,3.6,2)$ using 80 lattice sites and $\epsilon = 0.3/(2\pi)$, and (f) $(1,1,2,3)$. The black curve shows Eq. (16).

At $1/2 < \rho = 0.6 < 1$ [Fig. 2(iii)], we have case (II) with a broader $\mathcal{I}$ than $\rho = 1$. Compared to $\rho = 1$, the $N = 0$ region remains the same, but a neighborhood of the boundary of the $N = 1$ region has turned into an $N = 2$ region. A typical $N = 2$ dispersion relation computed using the pseudofield in Fig. 4(c) is shown in Fig. 3(e). Note that in this case, the predicted zero crossing on the right, say ω_r (shown in the inset), is quite close to the predicted value of ω_+. This implies that $P(\omega_r)$ is close to 1 and $\tilde{\alpha}(\omega_+)$ is close to 0. This is a sensitive case, so the number of lattice sites is increased to 80, and ϵ is decreased to $0.3/(2\pi)$. The numerical result is then in good agreement with the asymptotic prediction.
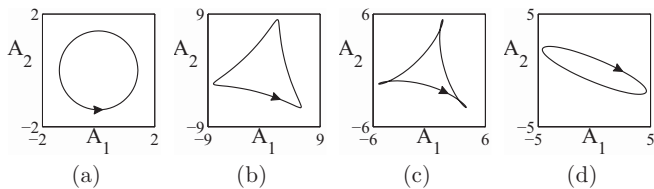

FIG. 4. Plots of the pseudofield $\mathbf{A}(\zeta) = (A_1(\zeta), A_2(\zeta))$ corresponding to the parameters used in (a) Figs. 3(a) and 3(c), (b) Figs. 3(b) and 3(d), (c) Fig. 3(e), and (d) Fig. 3(f).

At $\rho = 2 > 1$ [Fig. 2(iv)], we have case (II) with a narrower $\mathcal{I}$ than $\rho = 1$. Compared to $\rho = 1$, the $N = 0$ region has expanded, and correspondingly the $N = 1$ region has shrunk.

In the absence of the threefold symmetry, $\mathcal{I}$ should depend not only on ρ, but also on the pseudofield itself. Figure 2(v) shows a phase diagram computed using a twofold symmetric (or elliptic) pseudofield ($D = 1$). Indeed at $\rho = 1$, we have coexistence among cases (I)–(III). Interestingly, we find only $N = 2$ in the case (I) region and $N = 1$ in the case (II) region. A typical case (III) dispersion relation computed using the pseudofield in Fig. 4(d) is shown in Fig. 3(f).

We note that the difference between the $N = 1$ and the $N = 0, 2$ cases is distinguished by introducing a $\mathbb{Z}_2$ topological index, see Ref. [24], $I \equiv N \pmod 2$ such that the former (latter) situation corresponds to $I = 1$ ($I = 0$), namely, nontrivial (trivial) topology. We will explore this connection further in the future.

V. NONLINEAR TWO-DIMENSIONAL LOCALIZED EDGE MODES

Following the approach in Ref. [22] and comparing with experiments in Ref. [13], we construct 2D localized solutions by introducing an envelope in ω and taking the inverse Fourier transform in m. First we focus on fixed ω and modify our preceding analysis in Sec. III to account for weak nonlinearity where $\sigma = \epsilon\tilde{\sigma}$. The analysis proceeds as before, except that r_+ is replaced by $r_+ - \tilde{\sigma}|b^{(0)}|^2 b^{(0)}$ in Eq. (A1). In this case we arrive at the following equation:

$$i\,\partial_Z C = \tilde{\alpha}(\omega)C - \tilde{\sigma}\alpha_{nl}(\omega)|C|^2 C, \qquad (20)$$

where $\alpha_{nl}(\omega) = \|b^S\|_4^4 / \|b^S\|_2^2$ with

$$\|b^S\|_2^2 = \sum_{n=0}^{\infty} |b_n^S|^2, \quad \|b^S\|_4^4 = \sum_{n=0}^{\infty} |b_n^S|^4.$$

We can reconstruct the approximation to b_{mn} via

$$b_{mn} = C(Z, \omega)e^{i\omega m} b_n^S. \qquad (21)$$

In the narrow-band approximation with ω near any given $\omega_0 \in \mathcal{I}$, the solution C represents an envelope function with carrier wave number ω_0. To describe its dynamics, we first expand $\tilde{\alpha}(\omega)$ and $\alpha_{nl}(\omega)$ around ω_0. We then replace $\omega - \omega_0$ by $-i\nu\partial_y$, where ν is the width around ω_0 or the inverse width of the envelope in physical space. Finally, we rewrite Eq. (20) as the following equation for the envelope C:

$$i\,\partial_Z C = \left[\sum_{j=0}^{3} \frac{\tilde{\alpha}^{(j)}(\omega_0)}{j!}(-i\nu\partial_y)^j + O(\nu^4)\right] C$$
$$\qquad - \tilde{\sigma}[\alpha_{nl}(\omega_0) + O(\nu)]|C|^2 C, \qquad (22)$$

where $\tilde{\alpha}^{(j)}(\omega_0)$ denotes the jth derivative of $\tilde{\alpha}(\omega)$ at $\omega = \omega_0$. Equation (22) is a higher-order NLS equation.

There are interesting subcases. If $\tilde{\alpha}''(\omega_0) \neq 0$, then the equation is reduced at leading order to the well-known NLS equation given below,

$$i\,\partial_{\bar{Z}}\tilde{C} + \frac{\tilde{\alpha}''(\omega_0)}{2}\tilde{C}_{YY} + \sigma_{\text{eff}}|\tilde{C}|^2\tilde{C} = 0, \qquad (23)$$

where $C = \tilde{C}(Y,\tilde{Z})e^{-i\tilde{\alpha}(\omega_0)Z}$, $Y = y - v\tilde{\alpha}'(\omega_0)Z$, $\tilde{Z} = v^2 Z$, and $\sigma_{\text{eff}} = \tilde{\sigma}\alpha_{nl}(\omega_0)/v^2$. On the other hand if $\tilde{\alpha}''(\omega_0) = 0$, then the following "zero-dispersion" NLS equation is obtained

$$i\,\partial_{Z_3}\tilde{C} - i\frac{\tilde{\alpha}'''(\omega_0)}{6}\tilde{C}_{YYY} + \sigma_{z\text{eff}}|\tilde{C}|^2\tilde{C} = 0, \qquad (24)$$

where now $C = \tilde{C}(Y,Z_3)e^{-i\tilde{\alpha}(\omega_0)Z}$, $Y = y - v\tilde{\alpha}'(\omega_0)Z$, $Z_3 = v^3 Z$, and $\sigma_{z\text{eff}} = \tilde{\sigma}\alpha_{nl}(\omega_0)/v^3$.

As indicated above, Eq. (23) is the classical 1D NLS equation. The equation is maximally balanced when $\sigma_{\text{eff}} = O(1)$. In the focusing case $\tilde{\alpha}''(\omega_0)\sigma_{\text{eff}} > 0$, the NLS equation is known to contain solitons. Thus in this case the semi-infinite HC lattice truly contains edge solitons. In the defocusing case $\tilde{\alpha}''(\omega_0)\sigma_{\text{eff}} < 0$, the nonlinearity enhances dispersion, and so no soliton is expected. For the zero-dispersion NLS equation (24), which applies when $\tilde{\alpha}''(\omega_0) = 0$ and $\sigma_{z\text{eff}} = O(1)$, the nonlinearity also enhances dispersion somewhat.

To test these predictions, we solve the 2D discrete system Eqs. (8) and (9) numerically using the initial condition,

$$a_{mn} = 0, \quad b_{mn} = \int_{\mathcal{I}} \hat{b}(\omega) \frac{b_n^S(\omega)}{\sqrt{\langle b^S(\omega), b^S(\omega)\rangle}} e^{im\omega} d\omega, \quad (25)$$

where

$$\hat{b}(\omega) = \frac{e^{-(\omega-\omega_0)^2/v^2}}{\int_{\mathcal{I}} e^{-(\omega-\omega_0)^2/v^2} d\omega},$$

and compare the results with b_{mn} reconstructed from numerical solutions of the 1D NLS equation (22) with the initial condition,

$$C(Z = 0, y) = \int_{\mathcal{I}} \hat{b}(\omega) \frac{1}{\sqrt{\langle b^S(\omega), b^S(\omega)\rangle}} e^{iy(\omega-\omega_0)/v} d\omega. \quad (26)$$

In Fig. 5, we compare linear ($\sigma = 0$) edge modes found from the full 2D discrete system to those found from the 1D linear Schrödinger (LS) equation, i.e., Eq. (22) with $\tilde{\sigma} = 0$. The comparison of results is shown in terms of $|b_{m0}(z)|$. The left panels (a), (c), and (e) show the solutions of the 2D discrete system, and the right panels (b), (d), and (f) show the solutions of the 1D LS equation where we use the following modification of Eq. (21):

$$b_{mn} = C(Z, y)e^{i\omega_0 y/v} b_n^S \quad (27)$$

to reconstruct b_{mn} with C satisfying the LS equation.

In Fig. 6, we compare nonlinear ($\sigma \neq 0$) edge modes found from the full 2D discrete system to those found from the full 1D NLS equation (22). As before, the comparison of results is shown in terms of $|b_{m0}(z)|$, the left panels (a), (c), and (e) show the solutions of the 2D discrete system, and the right panels (b), (d), and (f) show the solutions of the 1D NLS equation with Eq. (27) used to reconstruct $|b_{m0}(z)|$.

In the absence of nonlinearity ($\sigma = 0$), the fastest and most robust unidirectional traveling mode is seen in Fig. 5(a), which corresponds to the $N = 1$ dispersion curve in Fig. 3(a) with $\tilde{\alpha}'(\omega_0) \neq 0$ [13]. In this case, relatively weak dispersion results from $\tilde{\alpha}''(\omega_0) = 0$, and the term $\tilde{\alpha}'''(\omega_0) \neq 0$ is a small higher-order contribution. Figures 5(c) and 5(e) both correspond to the $N = 2$ dispersion curve in Fig. 3(c) with $\tilde{\alpha}'(\omega_0) = 0$. In both cases, the linear dispersion resulting from $\tilde{\alpha}''(\omega_0) \neq 0$ essentially eliminates the mode after sufficient evolution.
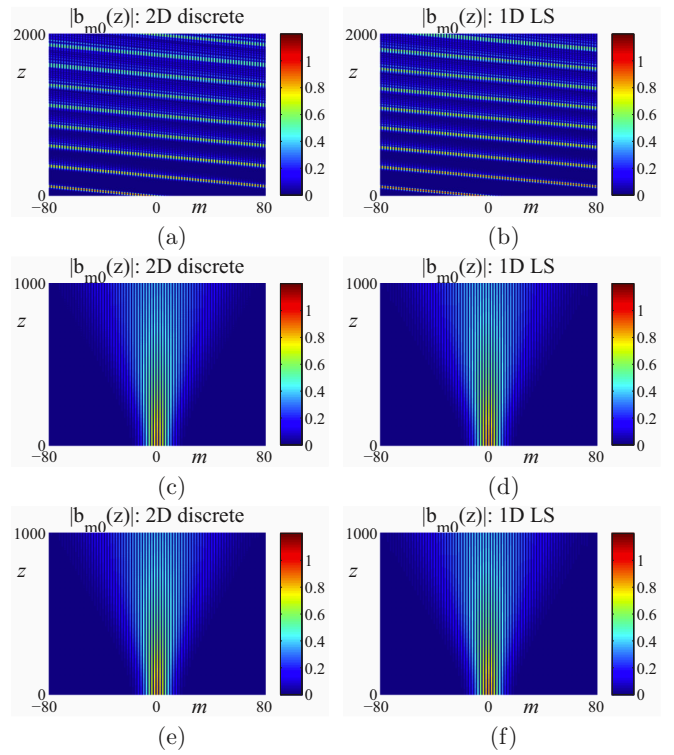

FIG. 5. (Color online) Plot of $|b_{m0}(z)|$ (at the edge) for parameters (ρ, v, ω_0): (a) and (b) $(1, 0.2, \pi/2)$, (c) and (d) $(0.4, 0.2, \pi/4)$, and (e) and (f) $(0.4, 0.2, 3\pi/4)$. The pseudofield parameters are fixed at $(D, \kappa, \lambda) = (2, 1.4, 0)$, and the edge modes are linear ($\sigma = 0$). Periodic boundary conditions in m are used. The left panels are calculated from the 2D discrete system Eqs. (8) and (9); the right panels are found from the 1D LS equation (22).

Figure 6(a) shows the nonlinear evolution using the same parameters as Fig. 5(a) but with $\sigma = 0.005 \sim \epsilon v^3$. Comparing these two panels, we see that the unidirectional traveling mode is largely maintained in the presence of weak nonlinearity, although dispersion is somewhat enhanced in the nonlinear case. Figures 6(c) and 6(e) show the nonlinear evolutions using the same parameters as in Figs. 5(c) and 5(e) but with $\sigma = 0.02 \sim \epsilon v^2$. For Fig. 6(c), which is described by the defocusing NLS equation, which has no solitons due to $\tilde{\alpha}''(\omega_0) < 0$, we see that weak nonlinearity enhances dispersion. On the other hand, for Fig. 6(e), which is described by the focusing NLS equation, which has solitons due to $\tilde{\alpha}''(\omega_0) > 0$, we see that weak nonlinearity enhances localization.

Comparing panels (b), (d), and (f) with panels (a), (c), and (e) in Figs. 5 and 6, we see that the 1D LS/NLS equation (22) reproduces the time evolution of the 2D discrete system (8) and (9) well up to $z \sim 1/(\epsilon v^3)$ for panel (a) and $z \sim 1/(\epsilon v^2)$ for panels (c) and (e). Beyond these time scales, higher-order terms must be added to Eq. (22) in order to explain, for example, the slow rightward drift of the wave envelope in Fig. 6(e).

Since solitons in the 1D focusing NLS equation are known to be stable, it is interesting to see how the edge solitons found above in the 2D discrete system propagate over long distances. Figure 7 shows two time evolutions computed using the same parameters as in Fig. 6(e), except that $\omega_0 = 5\pi/8$ and $\rho = 0.6$ for panel (a) and $\rho = 0.4$ for panel (b). Since $\tilde{\alpha}(\omega) \propto \rho^2$, it can
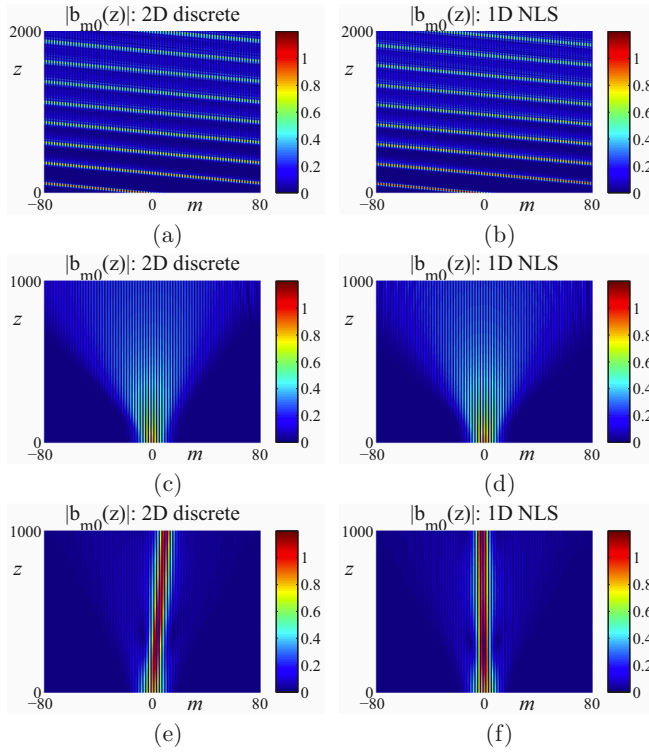
FIG. 6. (Color online) Plot of $|b_{m0}(z)|$ (at the edge) for the same parameters as in Fig. 5, except that (a) and (b) $\sigma = 0.005$; (c)–(f) $\sigma = 0.02$. The left panels are calculated from the 2D discrete system Eqs. (8) and (9); the right panels are found from the full 1D NLS equation (22) with $\tilde{\sigma} \neq 0$.

be seen from Fig. 3(c) that locally $\tilde{\alpha}'(\omega_0) \neq 0$ and $\tilde{\alpha}''(\omega_0) > 0$ in both cases and so the governing 1D NLS equation is focusing. The difference between these two choices of ρ is that globally the dispersion relation $\tilde{\alpha}(\omega)$ is topologically nontrivial [case (II), $N = 1$] for $\rho > 1/2$ and topologically trivial [case (I), $N = 2$] for $\rho < 1/2$. Over the distance $z \sim 1/(\epsilon \nu^2)$, the localized wave envelope indeed evolves into a traveling edge soliton in both cases as predicted by the NLS equation. However, for larger z, the edge soliton travels at a uniform velocity in Fig. 7(a) but gradually slows down due to backscattering in Fig. 7(b). This dramatic difference may be attributed to the fact that the linear topologically protected traveling edge waves, which are immune to backscattering,
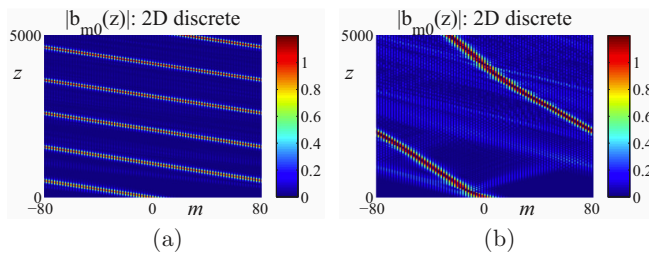

FIG. 7. (Color online) Plot of $|b_{m0}(z)|$ (at the edge) for the same parameters as in Fig. 6(e), except that $\omega_0 = 5\pi/8$ and (a) $\rho = 0.6$; (b) $\rho = 0.4$.

confer this immunity to nonlinear modes, such as the one in Fig. 7(a).

This immunity of traveling edge waves to backscattering in the topologically protected regime is usually explained in terms of the absence of counterpropagating edge modes. For this reason, these edge waves are also expected to be immune to backscattering and so maintain their topological protection in the presence of various types of disorder, at least for a degree of disorder below a certain threshold [7]. A detailed investigation of the dynamical behavior of traveling edge waves, using various types of disordered honeycomb lattices cf. Ref. [25], is a topic of interest but is outside the scope of the present study.

VI. CONCLUSION

In this paper, a method is developed which describes the propagation of edge modes in a semi-infinite honeycomb lattice in the presence of a periodically and relatively fast varying pseudofield and weak nonlinearity. In the linear case, various pseudofields are explored, and different dispersion relations are found to occur, some of which exhibit unidirectional wave propagation. A special case agrees with the results and experiments of Ref. [13]. With weak nonlinearity included, it is shown that in the narrow-band approximation, a higher-order NLS equation is obtained. Special cases include the classical NLS and zero-dispersion NLS equations. The classical NLS equation admits solitons, and they are found to be part of the long-time nonlinear evolution under suitable circumstances. This shows the existence of true edge solitons. Finally, over very long distances, with certain choices of parameters, consistent with the notion of topological protection as indicated by the linear-dispersion relation, localized nonlinear edge modes are found to be immune from backscattering, whereas with other choices of parameters, backscattering is observed.

APPENDIX A: ASYMPTOTIC ANALYSIS

With the method of multiple scales, we write the nth components of vectors a and b as

$$a_n = a_n(z, \zeta), \quad b_n = b_n(z, \zeta).$$

The coupled system given by Eqs. (10) and (11) then becomes

$$i\epsilon^{-1}\partial_\zeta a + i\,\partial_z a + \mathcal{L}^-(\zeta; \omega)b = 0,$$

$$i\epsilon^{-1}\partial_\zeta b + i\,\partial_z b + \mathcal{L}^+(\zeta; \omega)a = 0,$$

where the nth component of $\mathcal{L}^-(\zeta; \omega)b$ is

$$(\mathcal{L}^-(\zeta; \omega)b)_n = \varrho(\zeta)b_n + \vartheta(\zeta; \omega)b_{n-1},$$

the operator $\mathcal{L}^+$ is the Hermitian conjugate of $\mathcal{L}^-$, and

$$\varrho(\zeta) = e^{i\mathbf{d}\cdot\mathbf{A}}, \quad \vartheta(\zeta; \omega) = \vartheta_c(\zeta)\cos\omega + \vartheta_s(\zeta)\sin\omega,$$

$$\vartheta_c(\zeta) = \varrho(\zeta)2\rho e^{-i\varphi_+}\cos\varphi_-,$$

$$\vartheta_s(\zeta) = \varrho(\zeta)2\rho e^{-i\varphi_+}\sin\varphi_-.$$

Then we expand a_n, b_n in powers of ϵ,

$$a_n = a_n^{(0)} + \epsilon a_n^{(1)} + \cdots, \quad b_n = b_n^{(0)} + \epsilon b_n^{(1)} + \cdots.$$

At $O(\epsilon^{-1})$, $\partial_\zeta a_n^{(0)} = 0$ and $\partial_\zeta b_n^{(0)} = 0$, which leads to $a_n^{(0)} = a_n^{(0)}(z)$ and $b_n^{(0)} = b_n^{(0)}(z)$.

At $O(1)$, to remove secularities using the average $\bar{f} \equiv T^{-1} \int_0^T f(\zeta) d\zeta$, where T is the period of $\mathbf{A}$, we get

$$i\,\partial_z a^{(0)} + \bar{\mathcal{L}}^-(\omega) b^{(0)} = \epsilon r_-, \quad i\,\partial_z b^{(0)} + \bar{\mathcal{L}}^+(\omega) a^{(0)} = \epsilon r_+,$$
(A1)

where

$$r_- = -i\,\overline{\partial_z a^{(1)}} - \overline{\mathcal{L}^-(\zeta;\omega) b^{(1)}},$$
$$r_+ = -i\,\overline{\partial_z b^{(1)}} - \overline{\mathcal{L}^+(\zeta;\omega) a^{(1)}},$$
(A2)

and where $a^{(1)}$ and $b^{(1)}$ are found from

$$i\,\partial_\zeta a^{(1)} + (\mathcal{L}^-(\zeta;\omega) - \bar{\mathcal{L}}^-(\omega)) b^{(0)} = 0, \quad (A3)$$

$$i\,\partial_\zeta b^{(1)} + (\mathcal{L}^+(\zeta;\omega) - \bar{\mathcal{L}}^+(\omega)) a^{(0)} = 0. \quad (A4)$$

The zigzag boundary conditions imply $a_n(z,\zeta) = 0$, $n \leqslant 0$. As $\epsilon \to 0$, we have a stationary mode on the z scale so that $a_n^{(0)} = 0$ and $\overline{\mathcal{L}^-(\omega)} b^{(0)} = 0$. Thus to maintain asymptotic balance, for $\epsilon \neq 0$, this mode evolves on the Z scale where $Z = \epsilon z$, namely,

$$b^{(0)} = C(Z) b^S, \quad b_n^S = (-\bar{\vartheta}/\bar{\varrho})^n.$$

To eliminate secularities at the next order, we must have

$$iC^{-1}\partial_Z C = \langle r_+, b^S \rangle / \langle b^S, b^S \rangle \equiv \tilde{\alpha}, \quad (A5)$$

where $\langle \cdot, \cdot \rangle$ is the inner product between two vectors and r_+ is evaluated using Eqs. (A2)–(A4) with $a^{(0)} = 0$ and $b^{(0)} = b^S$. After introducing

$$Q(\zeta;\omega) \equiv \frac{(\mathcal{L}^-(\zeta;\omega) b^S)_n}{b_{n-1}^S} = -\varrho(\zeta)\frac{\bar{\vartheta}}{\bar{\varrho}} + \vartheta(\zeta;\omega), \quad (A6)$$

we see that $\tilde{\alpha}(\omega)$ becomes

$$\tilde{\alpha}(\omega) = -\frac{i}{T}\int_0^T \int_0^\zeta Q(\zeta';\omega) Q^*(\zeta;\omega) d\zeta' d\zeta. \quad (A7)$$

From Eq. (A6) we see that $\bar{Q} = 0$; using this fact it is shown in Appendix C that $\tilde{\alpha}$ is strictly real. Therefore the solution to Eq. (A5),

$$C(Z) = C(0) \exp(-i\tilde{\alpha}(\omega) Z) \quad (A8)$$

shows that the influence of the nontrivial pseudomagnetic field $\mathbf{A}(\zeta)$ on the stationary edge modes is the introduction of a nontrivial phase; as mentioned in Sec. III the function $\tilde{\alpha}(\omega)$ is identified as the dispersion relation.

APPENDIX B: RELATION BETWEEN THE DEFORMATION PARAMETER AND THE HONEYCOMB POTENTIAL

In this section, we study the dependence of the deformation parameter ρ on the honeycomb potential. The prototypical honeycomb potential used in this paper is (cf. Eq. (2) in Ref. [21])

$$V(\mathbf{r}) = V_0 \left[\frac{|e^{ik_0 \mathbf{b_1} \cdot \mathbf{r}} + \eta e^{ik_0 \mathbf{b_2} \cdot \mathbf{r}} + \eta e^{ik_0 \mathbf{b_3} \cdot \mathbf{r}}|^2}{(1 + 2\eta)^2} - 1 \right], \quad (B1)$$

where, $\mathbf{b_1} = (0,1)$, $\mathbf{b_2} = (-\frac{\sqrt{3}}{2}, -\frac{1}{2})$, $\mathbf{b_3} = (\frac{\sqrt{3}}{2}, -\frac{1}{2})$, $V_0 > 0$ is the potential strength, and η measures the relative strength of the second and third plane waves. To form a honeycomb lattice, $\eta > \frac{1}{2}$ must be satisfied; $\eta = 1$ corresponds to a perfect honeycomb.

In the Appendix to Ref. [21], the deformation parameter ρ is expressed in terms of the shift vectors $\mathbf{d}_s$, $s = 0$–2, from its three nearest B sites to an A site. The vectors $\mathbf{d}_s$ are functions of η; the vector $-\mathbf{d}_0$ is denoted by $\mathbf{d}$ in this paper. Near $\eta = 1$, the expression for ρ is at leading order,

$$\rho = e^{[(9+\sqrt{3}\pi)/18]\sqrt{V_0}(\eta-1)}, \quad (B2)$$

which can be solved as

$$\eta - 1 = \frac{18}{9 + \sqrt{3}\pi} V_0^{-1/2} \ln \rho. \quad (B3)$$

Near $\eta = 1$, the vector $\mathbf{d}$ becomes at leading order,

$$\mathbf{d} = \left(\frac{1}{\sqrt{3}} + \frac{1}{\pi}(\eta - 1), 0 \right). \quad (B4)$$

Therefore, when V_0 is large, as long as ρ is positive and not small, $\mathbf{d}$ changes little as a function of ρ.

APPENDIX C: THE REALITY OF THE DISPERSION RELATION

To show that $\bar{Q} = 0$ implies that $\tilde{\alpha}(\omega)$ given in Eq. (13) is real, we note that (parametric dependence of Q on ω is omitted for notational convenience),

$$T[i\tilde{\alpha}(\omega) + (i\tilde{\alpha}(\omega))^*]$$

$$= \int_0^T \int_0^\zeta Q(\zeta') Q^*(\zeta) d\zeta' d\zeta + \int_0^T \int_0^\zeta Q^*(\zeta') Q(\zeta) d\zeta' d\zeta$$

$$= \int_0^T \int_0^\zeta Q(\zeta') Q^*(\zeta) d\zeta' d\zeta + \int_0^T \int_\zeta^T Q^*(\zeta) Q(\zeta') d\zeta' d\zeta$$

$$= \int_0^T \int_0^T Q(\zeta') Q^*(\zeta) d\zeta' d\zeta = \left| \int_0^T Q(\zeta) d\zeta \right|^2 = 0.$$

[1] K. Klitzing, G. Dorda, and M. Pepper, Phys. Rev. Lett. **45**, 494 (1980).

[2] R. B. Laughlin, Phys. Rev. B **23**, 5632 (1981).

[3] D. J. Thouless, M. Kohmoto, M. P. Nightingale, and M. den Nijs, Phys. Rev. Lett. **49**, 405 (1982).

[4] B. Simon, Phys. Rev. Lett. **51**, 2167 (1983).

[5] A. Bohm, A. Mostafazadeh, H. Koizumi, Q. Niu, and J. Zwanziger, *The Geometric Phase in Quantum Systems* (Springer, Heidelberg, 2003).

[6] Y. Hatsugai, Phys. Rev. B **48**, 11851 (1993).

[7] M. Z. Hasan and C. L. Kane, Rev. Mod. Phys. **82**, 3045 (2010).

[8] D. Xiao, M. C. Chang, and Q. Niu, Rev. Mod. Phys. **82**, 1959 (2010).

[9] J. Zak, Phys. Rev. Lett. **62**, 2747 (1989).

[10] F. D. M. Haldane and S. Raghu, Phys. Rev. Lett. **100**, 013904 (2008).

[11] S. Raghu and F. D. M. Haldane, Phys. Rev. A **78**, 033834 (2008).

[12] Z. Wang, Y. Chong, J. D. Joannopoulos, and M. Soljacic, Nature (London) **461**, 772 (2009).

[13] M. C. Rechtsman, J. M. Zeuner, Y. Plotnik, Y. Lumer, S. Nolte, F. Dreisow, M. Segev, and A. Szameit, Nature (London) **496**, 196 (2013).

[14] A. Szameit and S. Nolte, J. Phys. B: At., Mol. Opt. Phys. **43**, 163001 (2010).

[15] J. B. Krieger and G. J. Iafrate, Phys. Rev. B **33**, 5494 (1986).

[16] M. C. Rechtsman, Y. Plotnik, J. M. Zeuner, D. Song, Z. Chen, A. Szameit, and M. Segev, Phys. Rev. Lett. **111**, 103901 (2013).

[17] T. Kitagawa, E. Berg, M. Rudner, and E. Demler, Phys. Rev. B **82**, 235114 (2010).

[18] N. H. Lindner, G. Refael, and V. Galitski, Nat. Phys. **7**, 490 (2011).

[19] Y. Lumer, Y. Plotnik, M. C. Rechtsman, and M. Segev, Phys. Rev. Lett. **111**, 243905 (2013).

[20] C. L. Fefferman, J. P. Thorpe, and M. I. Weinstein, arXiv:1405.4569.

[21] M. J. Ablowitz and Y. Zhu, Phys. Rev. A **82**, 013840 (2010).

[22] M. J. Ablowitz, C. W. Curtis, and Y. Zhu, Phys. Rev. A **88**, 013850 (2013).

[23] M. J. Ablowitz, *Nonlinear Dispersive Waves, Asymptotic Analysis and Solitons* (Cambridge University Press, Cambridge, UK, 2011).

[24] C. L. Kane and E. J. Mele, Phys. Rev. Lett. **95**, 146802 (2005).

[25] M. A. Kaliteevski, J. M. Martinez, D. Cassagne, and J. P. Albert, Phys. Rev. B **66**, 113101 (2002).